View metadata, citation and similar papers at core.ac.uk
brought to you by CORE
provided by NASA Technical Reports Server

N95-23839

THE EFFECT OF IMPACT ANGLE ON CRATERS FORMED BY HYPERVELOCITY PARTICLES

243-39

David C. Hill, M. Frank Rose, Steve R. Best, Michael S. Crumpler
Space Power Institute, 231 Leach Center
Auburn University, AL 36849
Phone (205) 844 5894; Fax (205) 844 5910

Gary D. Crawford & Ralph H-C. Zee
Department of Mechanical Engineering, 201 Ross Hall
Auburn University, AL 36849
Phone (205) 844 3320; Fax (205) 844 2672

Michael J. Bozack
Department of Physics, Allison Laboratory
Auburn University, AL 36849
Phone (205) 844 4264; Fax (205) 844 4613

SUMMARY

The Space Power Institute (SPI) at Auburn University has conducted experiments on the effects of impact angle on crater morphology and impactor residue retention for hypervelocity impacts. Copper target plates were set at angles of 30°, 45°, 60°, and 75° from the particle flight path. For the 30° and 45° impacts, in the velocity regime greater than 8 $km.s^{-1}$ the resultant craters are almost identical to normal incidence impacts. The only difference found was in the apparent distribution of particle residue within the crater, and further research is needed to verify this. The 60° and 75° impacts showed marked differences in crater symmetry, crater lip shape, and particle residue distribution in the same velocity regime. Impactor residue shock fractionation effects have been quantified to first-order. It is concluded that a combination of analysis techniques can yield further information on impact velocity, direction, and angle of incidence.

1 INTRODUCTION

Retrieval of LDEF, EURECA, and parts of Solar Max, from low Earth orbit (LEO) has allowed researchers to learn much about the space environment and its effects on spacecraft materials and structures. Within two years of the retrieval of LDEF, personnel of the Meteoroid & Debris Special Investigation Group (M&DSIG) had identified more than 34,000 features attributable to meteoroid and debris impacts. While it is unlikely, due to the low flux rates at higher masses, that the meteoroids or debris typically encountered by LDEF during its 5.75 year exposure could have caused catastrophic structural damage to a spacecraft, nevertheless, they may cause extensive damage to opti-

482

cal surfaces, solar cells, protective, anti-reflection and thermal control coatings, and other more delicate components or surfaces. Of extreme importance, currently, is the refinement of meteoroid and space debris environmental models in terms of particle masses, compositions, impact velocities, and directionality. This will allow better predictive capability and reliability in design optimization for spacecraft systems engineers.

A significant number of the impact sites identified to date by various researchers are on non-experimental and/or quasi-infinite flat surfaces. The implication of this is that impact angle of incidence (measured with respect to the surface normal) and azimuth (measured in the plane of the target surface) can only be deduced from the morphology of the resultant impact site. Several researchers (Paul, 1993; Mackay *et al.*, 1993; Newman *et al.*, 1992) have emphasized the need to determine incidence and azimuth angles (where possible) for transformation into impact vectors in the LDEF body reference frame so that limits on the impactor orbital parameters can be placed. Additionally, the application of impactor residue chemical analysis, utilizing energy dispersive X-ray spectrometry (EDXS) and/or secondary ion mass spectrometry (SIMS), has been demonstrated to be useful in deducing the relative flux rates of debris and meteoroid particles by numerous authors (Berthoud *et al.*, 1993; Hörz *et al.*, 1993; Simon *et al.*, 1992).

The qualitative effects of impact angle on the cratering process have been elaborated by many researchers (Summers & Charters, 1958; Summers, 1959; Kineke, 1960; Bruce, 1961; Gehring & Lieblein, 1963; Nysmith & Summers, 1962). More recent investigations in the LDEF context were conducted by Newman *et al.* (1992), who provided a basis for the derivation of directional information from analysis of "elliptical" impact craters. In general, the crater which is formed by a normal or near-normal incidence hypervelocity impactor is roughly hemispherical (figure 1). Deviations from this originate in the relationship between impact velocity, impactor/target materials combination, and angle of incidence. For example, if the normal component of velocity for an oblique impact is sufficiently high the resultant crater remains hemispherical. As the normal component of velocity decreases with increasing obliquity, the crater geometry formed departs from that characteristic of normal incidence, exhibiting a hybrid circular-elliptic "footprint" at the target surface and an asymmetric circular-elliptic profile along the impact axis (figure 2).

This paper describes a series of experiments to begin the quantification of oblique impact phenomena. Since there is little previous work on impact obliquity at impact velocities greater than 8 $km.s^{-1}$, it was decided to investigate the 7-13.5 $km.s^{-1}$ impact velocity regime using 20-100μm diameter impactors. In the context of LDEF impact sites, where impact angle and azimuth are unknown, the question arises; *"is it possible to place bounds on impact angle and velocity from a combination of crater shape and residue location?"* The resulting objectives of this program are threefold: (i) to reproduce impact sites in the laboratory typical of LDEF impact sites on quasi-infinite metallic surfaces, (ii) to correlate distinctive morphological aspects of crater structure with impact velocity and angle of incidence, and (iii) to locate and analyze the amount and structure of particle residues as functions of impact velocity and angle.

Observations of crater morphology as a function of angle of incidence and impact velocity were made. EDXS techniques were employed to determine the location and abundance of residues, leading to the suggestion that crater interior residue location is

also useful in extracting information about impact angle of incidence and azimuth, particularly in the case of craters showing near-circular footprints or no cross-sectional asymmetry along the direction of impact.

2 EXPERIMENTS

The Hypervelocity Impact Facility (HIF), a plasma-drag accelerator, at SPI was used for these experiments. Rose *et al.* (1992) provide a description of the HIF system and its performance capabilities. Two pre-cursor test shots were executed, the first shot with the target plate surface normal set at an angle of 30° to the particle flight path, and the second set at 60°. Under this protocol a "0° impact" is at normal incidence whilst a "90° impact" is at grazing incidence.

Olivine particles (75 μm nominal diameter), having the chemical composition $(Mg:Fe)_2SiO_4$ and a Mg:Fe:Si ratio of ~19:1:10, were launched at copper targets. Olivine, although higher in density than that usually accepted for meteoroids (ρ = 0.5-1.5 $g.cm^{-3}$), was chosen as the best meteoroid simulant material that can be accelerated in the HIF system. Note that the mass density of olivine is 3.21 $g.cm^{-3}$ and that of copper is 8.92 $g.cm^{-3}$, resulting in a mass density ratio of ~0.36. This figure corresponds to that for low density (ρ ~ 1 $g.cm^{-3}$) meteoroids impacting aluminum (ρ ~2.7 $g.cm^{-3}$) targets. It should be remembered that the density ratio scaling between different materials combinations is a first order approximation only. Peak impact pressure, post-shock mass velocity, and shock velocity all play rôles that will lead to deviations from density ratio scaling at second order level.

A thin Mylar® film (thickness 0.5 μm) was placed in front of the target plates, such that it was always normal to the particle flight path. The hypervelocity particles pass through the film before striking the plate, allowing the particle size to be found (Carey *et al.*, 1984; Rose *et al.*, 1992). The film also minimizes gun debris contamination of the target surface.

Impact velocity is determined by observing the impact-induced plasma flash with an image converter camera (Hadland Photonics IMACON 790), operating in streak mode. The camera is aligned such that its optical axis is parallel to, and displaced approximately 0.1 mm from, the target surface. Its field-of-view is constrained to a width of ~0.5 mm by an entrance slit, whose image is "streaked" across the film plane at a known rate.

By means of a mirror inclined at 45° with respect to the optical axis both the X- and Y-location of the impact flash may be determined since the optical system produces two images of the flash, vertically displaced positively (X) and negatively (Y). The horizontal position of the twin flash events on the film uniquely determines the impact velocity. Modulated LEDs are placed at the corners of target area to allow easy determination of the X-Y co-ordinates and to facilitate the measurement of the time of impact. Rose *et al.* (1992) describe the diagnostics in detail with schematic diagrams.

Four experimental hypervelocity impact shots were executed, from which resulted in excess of 200 impact sites, identified using an optical scanning system. The minimum

identifiable site diameter was ~5 μm. The X-Y locations of all the sites were logged for subsequent correlation with streak record data. Shot D76 (normal incidence) was conducted to confirm gun performance and to determine the typical morphological structures that could be expected for olivine-copper impacts.

For the purposes of this paper, we selected thirteen impact sites from the four shots for detailed analysis. These, listed below in table 1, are representative of the numerous impact sites observed. Olivine residue was present in all of the selected craters, implying that residue retention can be expected at normal components of impact velocity up to 12 $km.s^{-1}$ for the materials combination used in this set of experiments, and also for meteoroids striking aluminum targets if density ratio scaling is assumed to hold. Preliminary modeling of the flux dynamics of flat plates exposed to an *isotropic* meteoroid flux distribution (with the Erickson velocity distribution) indicates that at least 12% of meteoroid craters on the RAM (East) surface should retain residue at levels detectable using EDXS, while at least 65% of WAKE (West) surface craters should retain similar residue. These numbers should be regarded as order of magnitude computations at present.

Site #	**Angle** [deg]	**Velocity** [$km.s^{-1}$]	**Residue Appearance**
D76-01-17	0	2.9	white, granular, crystalline
D76-01-16	0	4.8	white, granular, crystalline
D76-03-10	0	3.0	white, granular, crystalline
D76-03-13	0	9.9	transparent, glassy
D76-05-04	0	8.0	white, granular, crystalline
D76-05-05	0	9.6	transparent, glassy
D76-05-26	0	12.0	transparent, glassy
D76-05-32	0	12.0	transparent, glassy
D80-05-123	45	10.5	transparent, glassy
D78-05-23	60	8.5	white, granular, crystalline
D78-03-17	60	10.5	transparent, glassy
D79-01-02	75	5.7	white, granular, crystalline
D79-03-04	75	12.5	white, granular, crystalline

Table 1. *Sites selected for detailed SEM and EDXS analysis.*

The normal incidence shot (D76) also provided a baseline for analyzing the residue structure within the craters. Two residue types manifested themselves in this set of craters: white, granular, crystalline; and transparent, smooth, glassy (amorphous). These morphologies are impact velocity dependent, the granular structures being evidence of lower shock intensity while the glassy residue results from shock-induced melting and re-solidification processes. Further discussion of the residue structures and relative elemental compositions follows in sections 3 and 4 below.

3 CRATER MORPHOLOGIES

3.1 Pre-cursor Test Shots

For the analysis of both the 30° and 60° pre-cursor test shot impact sites, a JEOL 840 scanning electron microscope (SEM) with an EDXS sub-system was used. Figure 3 shows a typical crater caused by an olivine particle. The particle velocity was 7.0±0.05 $km.s^{-1}$ and the crater shape is fairly typical of all the craters analyzed. The crater is practically indistinguishable from normal incidence impacts, exhibiting a circular "footprint" and a roughly hemispherical profile with a depth-to-diameter ratio (p/D) of 0.43. The circumferential lip has no characteristics which hint at the direction of tilt of the target plate. The arrow at the bottom left-hand corner of the photomicrograph shows the direction of the component of the impact velocity vector in the plane of the target.

The entire interior of the crater is covered with olivine residue, and the granules inside the crater are "chunks" of olivine. Upon closer qualitative inspection, more olivine residue was located on the trailing interior surface of the crater than on the leading interior surface. This phenomenon was found in all of the olivine craters analyzed.

There is a marked difference between the 60° impacts and the 30° impacts. The main characteristics, shown in figure 2, were as follows: firstly, there is a minimal lip on the crater leading edge whereas an extensive lip was found on the trailing edge; secondly, significantly more particle residue was found on the trailing interior surface; and thirdly, the crater rims were "elliptical" rather than circular in shape.

Figure 4 shows a typical 60° angle of incidence impact crater, formed by an olivine particle traveling at 5.6 $km.s^{-1}$. Note how the crater lip becomes progressively smaller as the leading edge is approached, until it is practically non-existent at the apex of the leading edge. This crater has a coating of olivine throughout the crater interior surface, and a few grains of olivine are also evident. The p/D ratio along the minor axis is 0.30, and is 0.18 along the major axis, with a crater depth of 14 μm. There are more olivine grains located on the trailing interior surface than on the leading surface.

Another very interesting phenomenon seen on some of the 60° impact sites is the presence of small "indentations," some containing small amounts of olivine residue, downrange of the trailing edge crater lip. Clearly, the angle of incidence is such that some material from the top of the impactor has decoupled from the main body of the impactor during the impact and followed a trajectory that passes over the top of the trailing edge crater lip (in process of forming) before striking the target surface downrange of that lip.

Figure 5 shows a 60° impact crater formed by a particle traveling at 4.7 $km.s^{-1}$. It has the same lip asymmetry and residue distribution as the crater shown in figure 4, although its rim is more circular than elliptical. The crater is 43 μm deep at its deepest penetration point, with a minor axis p/D ratio of 0.28. Note that the p/D ratio for olivine particles striking a copper plate for normal incidence impact is between 0.50 and 0.38 in the velocity regime studied, *i.e.* ~3 - 12.5 $km.s^{-1}$.

3.2 Main Experimental Shots

For the purposes of this paper, we selected two representative normal incidence impact sites for more extensive morphological analysis. Site D76-01-17 (figure 6) is a 184±3μm diameter crater, with a circular footprint and raised circumferential lips, exhibiting a p/D ratio of 0.42±0.02, computed from a measured depth of 77±3μm. The impact velocity was 2.9±0.05 km.s^{-1}. Coating the interior of this crater was a whitish-green (when viewed optically) granular residue. Conversely, the lips of this crater were coated with a smooth, glassy residue, typical of that found in the interiors of the impact craters produced by faster impactors.

At the other end of the velocity spectrum is site D76-05-26 (figure 7), produced by an olivine fragment traveling at 12.0±0.05 km.s^{-1}. Again, the circular footprint and raised circumferential lips of a hypervelocity impact are evident. The p/D ratio was computed to be 0.47±0.08 from a crater diameter (D) of 38±2μm and a depth of 18±2μm. The interior of this crater was coated with a smooth, glassy residue, transparent when viewed optically.

The normal incidence crater set was characterized by a division into predominantly granular residues and predominantly glassy residues occurring at an impact velocity of between 8.0 km.s^{-1} and 9.6 km.s^{-1}, which corresponds to a shock pressure of between 185 GPa and 240 GPa, using a computational scheme similar to that used by Ang (1990). The implications of this, for site D76-01-17, is that the impactor residue in the crater interior, in granular form, has undergone a significantly less intense shock metamorphosis than that deposited on the crater lips. It is not clear from the data available from this analysis at what shock pressure threshold the transition from crystalline to amorphous residues occurs.

To obtain a preliminary quantitative idea of the effects of impact obliquity on various crater parameters, we selected five oblique impact sites for further detailed analysis. Data pertaining to these craters are tabulated in table 2, below.

Site #	Diameter [μm]	Depth [μm]	p/D	Velocity [km.s^{-1}]	Angle [deg]
D78-03-17	42±2	17±2	0.40±0.07	10.5±0.5	60
D78-05-23	60±2	19±2	0.32±0.04	8.5±0.5	60
D79-03-04	56±2	25±2	0.45±0.05	12.5±0.1	75
D79-01-02	n/d	n/d	n/d	5.7±0.1	75
D80-05-123	63±2	30±2	0.48±0.05	10.5±0.5	45

Table 2. *Crater parameters of sites selected for further EDXS analysis. The depth is measured at the deepest point and the diameter is measured perpendicular to the impact trajectory axis at that point. Note that for site D79-03-04 the depth is at the deepest point of the major crater.*

Figure 8 shows a deep (p/D = 0.40) crater impact site (D78-03-17) with a circular-elliptical surface footprint. The leading edge lips are less pronounced and more irregular than the trailing edge lips. The crater interior is coated with a smooth, glassy (amorphous) olivine residue over most of the interior surface, but with additional granular deposits in the deepest part of the crater and across the leading edge wall. The normal component of impact velocity is 5.3±0.3 km.s^{-1}, the angle of incidence being 60°.

Figure 9 shows a slightly larger, but more shallow (p/D = 0.32) and more elliptical, crater (D78-05-23), produced during the same experimental shot. The normal component of velocity was computed to be 4.3±0.3 km.s^{-1}, which correlates well with that of D78-03-17 where the higher normal component of velocity produced a deeper crater. The impactor residue appears to be smooth and glassy with few granular elements, suggesting that in this impact velocity regime, 8-11 km.s^{-1}, for oblique incidence, the degree of shock processing of impactor material is a probabilistic process, with both types of residue being present in varying (and unpredictable) relative amounts. This regime can be considered as a transition regime for the olivine-copper system in terms of shock processing. At higher normal component velocities the residue should manifest itself as smooth and glassy (amorphous), whereas at lower velocities the residue is whitish-green and granular (crystalline).

Figure 10 shows impact site D80-05-123, a 45° incidence impact with a velocity of 10.5±0.5 km.s^{-1}. The normal component is computed to be 7.4±0.4 km.s^{-1}. In this case, the crater exhibits a p/D ratio of 0.48 and has a near-circular surface footprint, almost indistinguishable from a normal incidence crater. Residue is almost entirely of the smooth and glassy type, although a few granular structures manifest themselves at higher magnifications. The leading edge lip is of similar extent to the trailing edge lip, except for the large petal in the lower left corner. It is possible that there is some correlation between impact direction and this pronounced structure on the trailing edge, but more evidence is necessary for conclusive proof. It should be borne in mind, though, that it is extremely rare for such asymmetry of lip-petal size to occur for normal incidence impacts.

Taking the oblique impact scenario to an extreme case, we executed one shot for 75° angle of incidence. Two impact sites, D79-01-02 and D79-03-04, were selected, the former representative of the lower (5.7 km.s^{-1}) velocity limit and the latter representative of the upper (12.5 km.s^{-1}) limit for this experiment. These are shown in figures 11 and 12, respectively. For the low velocity impact (normal component = 1.5±0.01 km.s^{-1}) the impactor embedded itself progressively as evidenced by the gouge uprange of the major crater, and then fragmented, leaving downrange impactor residue. The interior of the major crater (center of figure 11) contained granular residues similar to that found in the impact sites analyzed above. Both uprange and downrange impact damage areas also contained olivine residue. Although granular residue features were absent from these locations, we are reluctant to classify the residue as smooth and glassy, as for the higher velocity impact sites, since these surfaces are dominated by substrate (copper target) roughness, most likely artifacts from the impact gouging process.

The final site under analysis for this paper is D79-03-04. The normal component of velocity in this case was 3.2±0.01 km.s^{-1}. The photomicrograph reveals a major crater, having the circular-elliptic footprint typical of 30-45° incidence impacts, and significant

downrange impact damage. Similar to the 60° impacts at lower velocities reported above, the major crater has minimal leading edge lips, more pronounced trailing edge lips, and a p/D ratio of 0.45 at the deepest penetration point. Clearly, the top of the impactor has sheared off during the later stages of the impact, due to the shock front interaction with the impactor rear surface, and the respective trajectories of the fragments have taken them over the trailing edge lips to impact the target surface downrange of the main crater. The transverse component of impact velocity (parallel with the impact direction) is 12.1 $km.s^{-1}$, which is obviously sufficient to cause extreme shear stresses in the impactor. Granular residues were observed in the major crater, embedded in a glassy residue. No grains were observed in the downrange damage sites, although the EDXS analysis (see following section) does reveal significant olivine residue.

4 IMPACTOR RESIDUE ANALYSIS

To further understand the effects of impact obliquity and to provide support for the analysis of impact craters recovered from space-exposed quasi-infinite target surfaces, it is necessary to consider the abundance and distribution of impactor residues in the resultant craters. We, therefore, have begun a program of impactor residue analysis using EDXS techniques. Samples on which hypervelocity craters were produced were placed in an SEM (Cambridge StereoScan 200) and the X-ray spectrum, derived from the excited states of the atoms present in the target/residue materials, was measured using an EG&G Ortec System 5000 X-ray spectrum analyzer. Compositional calculations were done using the SEM community-standard AutoZAP II program.

For all analysis runs the accelerating voltage was set at 20 kV, which allowed the substrate (copper) signal to become significant. Elapsed live time was 100.00 seconds and the beam current varied from 0.3 nA to 4.6 nA. In all cases the specimen tilt angle was 45.0 degrees with respect to the X-axis and 0.0 degrees with respect to the Y-axis. Insertion depth was 60.0 mm with a typical working depth of between 15-19 mm.

We present quantitative data (see table 3), corrected for substrate contamination, from which relative abundances of elements can be computed for each of the craters. Careful orientation of the crater with respect to the electron gun axis and the X-ray detector minimizes the geometric effects of deep craters. For normal incidence impacts location (1) is on the crater inner side wall and location (2) is on the crater lip. For oblique impacts (D78 and D80 sites) location (1) is situated on the leading edge inner side wall and location (2) is on the trailing edge inner side wall. For D79 sites, locations (2) and (3) are in the downrange damage areas beyond the main crater trailing edge.

The first trend to consider is that between the location (1) analyses, excluding D80-05-123 which results in significantly anomalous data. Normal component of impact velocity (V_n) correlates directly with residue Mg:Si ratio (figure 13), implying shock-induced fractionation, i.e. the higher the velocity the more silicon is removed from the material matrix. This effect is confirmed by the appearance of the residue, as noted in section 3.2 above, *i.e.* the whitish-green granular residues are the least shock-fractionated (low Mg:Si ratio), whereas the smooth, glassy residues are the most shock-fractionated (high Mg:Si ratio).

Also, residue percentage (RES%), determined by computing the ratio of residue (Mg, Si & Fe) counts to total counts (Mg, Si, Fe & Cu) for location (1) data shows correlation with normal component of velocity (V_n), with the highest velocities producing the lowest residue percentage, *i.e.* the residue layer thickness is apparently reduced for higher velocities (see figure 14). A further consideration of the ratio of location (1) residue percentage to location (2) residue percentage for impact sites D78-03-17 and D80-05-123 indicates that for oblique angles of incidence more residue tends to be found on the trailing interior surface than the leading interior surface for craters with glassy, amorphous residues. The degree of downrange displacement appears to correlate with V_n with higher normal components of impact velocity producing more displacement. Consideration of the residue ratio (0.9±0.2) for site D78-05-23 shows that for sites with the white, granular, crystalline residue there is no apparent displacement of residue in the downrange direction.

SITE #	Mg	Si	Fe	Cu	Mg:Si	RES%	V_n	(2):(1)
D76-05-26(1)	17.6	5.4	1.1	75.9	8.7	21	12.0	n/a
D76-01-17(1)	28.8	11.0	2.0	58.2	3.4	39	2.9	n/a
D76-01-17(2)	18.7	5.4	0.4	75.5	9.2	22	-	-
D78-03-17(1)	23.7	6.9	2.4	67.0	6.1	30	5.3	1.4±0.2
D78-03-17(2)	33.7	10.9	0.9	54.5	4.0	43	-	-
D78-05-23(1)	25.0	7.3	0.9	66.8	5.8	30	4.3	0.9±0.2
D78-05-23(2)	20.1	8.2	1.4	70.3	4.0	27	-	-
D79-03-04(1)	30.1	10.0	1.7	58.2	4.1	39	3.2	n/a
D79-03-04(2)	23.8	8.1	0.9	67.2	4.7	30	-	n/a
D79-03-04(3)	18.5	5.6	0.5	75.4	8.3	21	-	n/a
D79-01-02(1)	39.5	17.1	2.1	41.3	2.6	57	1.5	n/a
D79-01-02(2)	23.2	7.4	0.9	68.5	5.3	28	-	n/a
D79-01-02(3)	20.4	2.9	0.5	76.2	n/a	23	-	n/a
D80-05-123(1)	15.9	3.9	1.3	78.9	41.8	20	7.4	2.1±0.4
D80-05-123(2)	29.1	10.4	0.7	59.8	3.8	41	-	-

Table 3. *Significant elemental composition by atomic percentage, Mg:Si ratio, and the residue percentage of the total sample. Substrate Si contamination counts were corrected for to obtain the Mg:Si ratio using the measured substrate atomic percentages , i.e. Si=4.27%, Cu=95.73%.*

We were careful to conduct several EDXS analyses for the specified general locations in order to eliminate any localized variations in relative elemental abundances that may be present. It is clear from these preliminary experiments that impact angle definitely affects the degree of shock-fractionation experienced by the impactor material and also the relative amounts of residue as a function of location. Effectively, two processes are at work: firstly, shock-fractionation; and, secondly, the displacement of the residue in the downrange direction as a function of the normal component of impact velocity. With this limited data set we are unable to provide a more detailed insight at present, but we are confident that further experiments will result in a better quantification of the residue location as a function of impact velocity and impact angle.

5 CONCLUSIONS

The results obtained to date suggest that a combination of crater morphology and residue analysis can give evidence of impact azimuth even when the crater profile is near hemispherical as in the case of 30° - 45° impacts. Also, lip structure correlation with impact azimuth, even for impacts in the 0° to 45° range, may be possible. The complex mechanics in oblique impacts where the residue is displaced downrange and undergoes variations in shock fractionation as a function of position have begun to be unraveled. In particular, relative amounts and locations of residue do correlate with impact velocity and can provide limits on that velocity. It is concluded that a combination of analysis techniques can yield further information on impact velocity, direction, and angle of incidence. It remains to be seen whether these findings can be used for LDEF crater analysis where the impact velocities are higher (15-25 $km.s^{-1}$) and residues can only be detected by other techniques such as SIMS.

6 FUTURE WORK

Recognizing the limitations of this work to date, we shall continue to execute hypervelocity impact shots to move from a semi-qualitative analysis with some quantitative indicators to a more quantitative basis. We expect to execute shots using olivine, glass, and polystyrene impactors striking Al1100 and Al6061 targets. These experiments will access lower density impactor phenomena.

7 ACKNOWLEDGMENTS

This work was supported by NASA Langley Research Center under grant number NAG-1-1329, which we gratefully acknowledge. We also thank Don Humes for reviewing this paper and suggesting improvements.

8 REFERENCES

Ang, J.A. (1990). *Int. J. Impact Eng.*, **10**, 1-4, pp23-34.
Berthoud, L. *et al.* (1993). *3rd LDEF Post-Ret. Symp. Abstr.*, pp58, NASA CP-10120.
Bruce, E.P. (1961). *Proc. 5th Symp. Hypervel. Impact,* Denver, CO.
Carey, W.C. *et al.* (1984). *Proc. 85th Coll. Int. Astron. Union Meeting,* Paper B.5.
Gehring, J.W. & Leiblein, S. (1963). *Prog. Astronaut. & Aeronaut.*, vol. 11.
Hörz, F. *et al.* (1993). *3rd LDEF Post-Ret. Symp. Abstr.*, pp57, NASA CP-10120.
Kineke, J.H. (1960). *Proc. 4th Symp. Hypervel. Impact,* Eglin AFB, FL.
Mackay, N.G. *et al.* (1993). *3rd LDEF Post-Ret. Symp. Abstr.*, pp67, NASA CP-10120.
Newman, P.J. *et al.* (1992). *Proc. 2nd LDEF Post-Ret.Symp.*, pp417-30, NASA CP-3194.
Nysmith, C.R. & Summers, J.L. (1962). NASA TN-D-1431.
Paul, K. (1993). *3rd LDEF Post-Ret. Symp. Abstr.*, pp67, NASA CP-10120.
Rose, M.F. *et al.* (1992). *Proc. 2nd LDEF Post-Ret. Symp.*, pp479-92, NASA CP-3194.
Simon, C.G. *et al.* (1992). *Proc. 2nd LDEF Post-Ret. Symp.*, pp677-92, NASA CP-3194.
Summers, J.L. (1959). NASA TN-D-94.
Summers, J.L. & Charters, A.C. (1958). *Proc. 3rd Symp. Hypervel. Impact,* Chicago, IL.

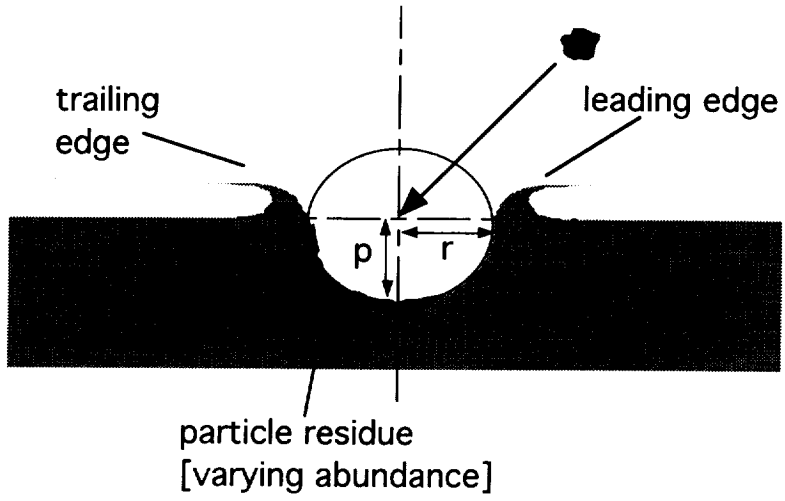

Figure 1. *Schematic of idealized profile of normal-to-45° oblique incidence hypervelocity impact crater. The penetration depth (p) and crater radius (r) are related to the particle diameter (d) and normal component of velocity (v_n) similar to the relationship between penetration depth, particle diameter and impact velocity for normal incidence impacts.*

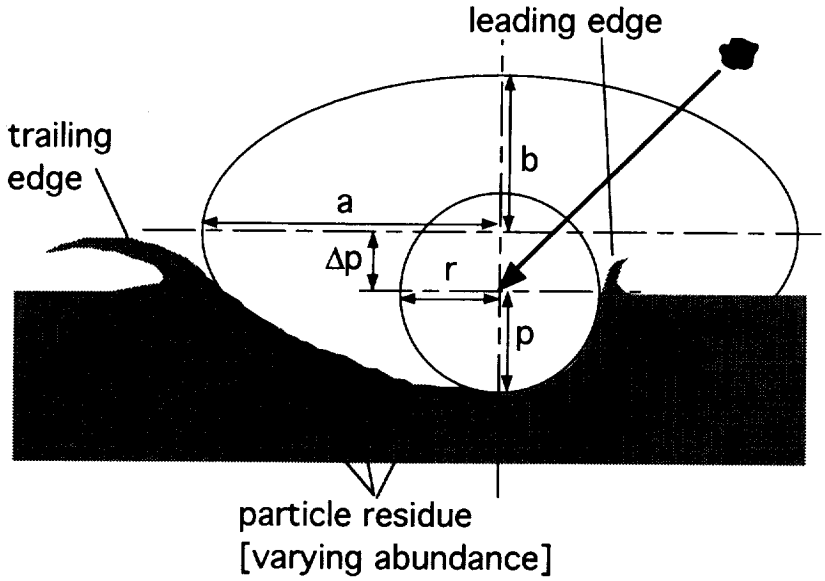

Figure 2. *Schematic of idealized profile of 45°-to-60°oblique hypervelocity impact crater. The minor ellipse (circle, in this case) parameters, penetration depth (p) and crater radius (r) are related to the particle diameter (d) and normal component of velocity (v_n) similar to the relationship between penetration depth, particle diameter and impact velocity for normal incidence impacts. The major ellipse parameters (a), (b), and (Δp) should be related to the angle of incidence and the shock propagation velocity in the target material.*

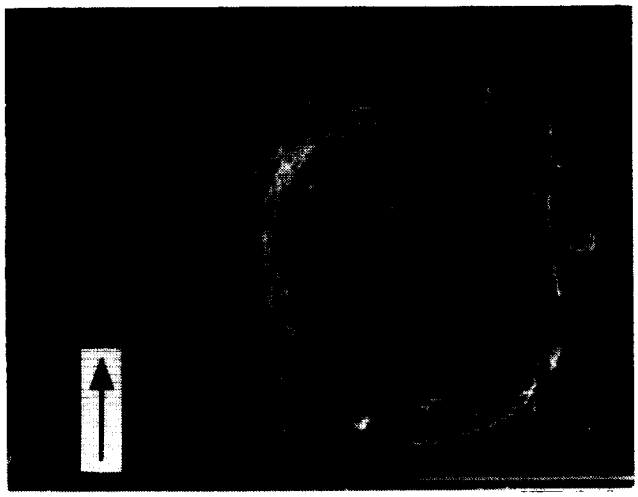

Figure 3. *Photomicrograph of an impact site formed by an olivine particle impacting with a velocity of 7.0 km.s^{-1} at an angle of 30° w.r.t. surface normal. Impact direction is indicated by the arrow. Olivine coating throughout the interior, with visible particle grains. Note the circular footprint and symmetrical lips. [scale bar = 100 μm]*

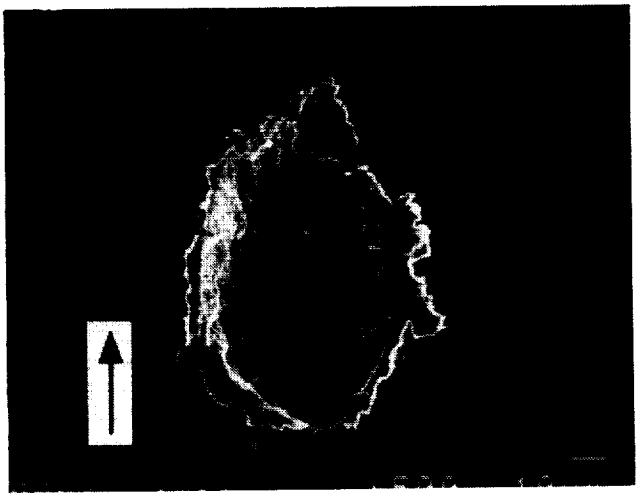

Figure 4. *Photomicrograph of an impact site formed by an olivine particle impacting with a velocity of 5.6 km.s^{-1} at an angle of 60° w.r.t. surface normal. Impact direction is indicated by the arrow. Note the "elliptical" footprint and lip asymmetry between the leading (lower) edge and the trailing (upper) edge. [scale bar = 10 μm]*

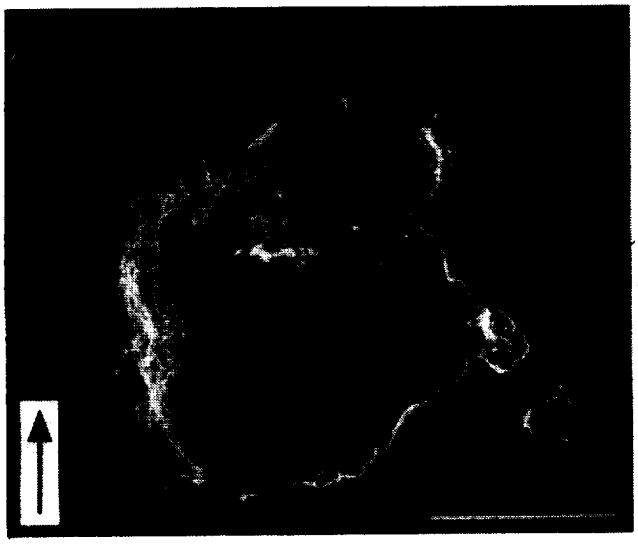

Figure 5. *Photomicrograph of an impact site formed by an olivine particle impacting with a velocity of 4.6 km.s^{-1} at an angle of 60°. Impact direction is indicated by the arrow. Note the "elliptical" footprint and lip asymmetry between the leading (lower) edge and the trailing (upper) edge. Also, note the non-uniformity of the impactor residue, with more residue being located toward the trailing edge of the crater. Some fragmentation damage downrange of the trailing lip is also visible. [scale bar = 100 μm]*

ORIGINAL PAGE IS
OF POOR QUALITY

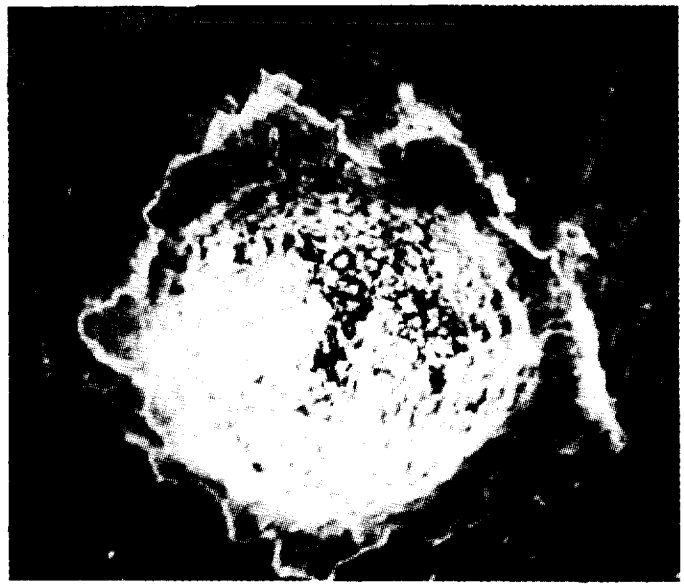

Figure 6. *Photomicrograph of impact site D76-01-17. Impact velocity is 2.9 km.s^{-1} and angle of incidence is normal to the target surface Note the circular "footprint" and symmetrical raised circumferential lips. Since this site was imaged in the SEM without a conductive coating the granular residue typical of lower velocities has saturated the film due to surface charging. It is interesting to note that such residues in craters could provide charging sites in the LEO plasma environment on surfaces regarded as pristine (and not subject to charging) prior to flight.*

Figure 7. *Photomicrograph of impact site D76-05-26. Impact velocity is 12.0 km.s^{-1} and angle of incidence is normal to the target surface. Again, note the circular "footprint" and symmetrical raised circumferential lips. By comparison to figure 6 there is no evidence of residue charging in the SEM electron beam, even though a glassy, transparent residue was detected using EDXS. This residue was more highly shock-processed with a Mg:Si ratio of 8.7, compared to 3.4 for the interior of site D76-01-17.*

ORIGINAL PAGE IS
OF POOR QUALITY

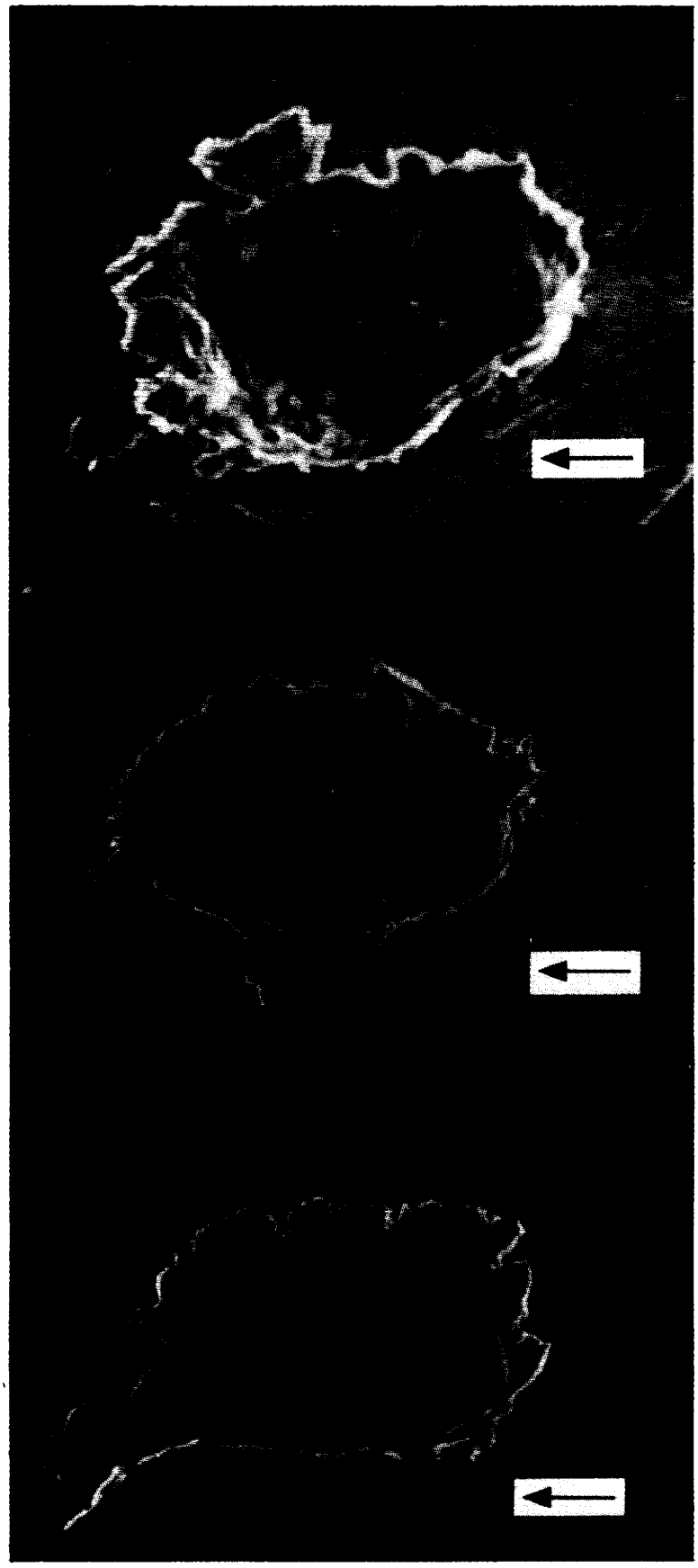

Figure 8. *Photomicrograph of impact site D78-03-17. Impact velocity was 10.5 km.s^{-1} and angle of incidence is 60° (w.r.t. surface normal). Impact direction is indicated by the arrow. Note the granular residue and pronounced trailing edge lips. p/D ratio is 0.40.*

Figure 9. *Photomicrograph of impact site D78-05-23. Impact velocity was 8.5 km.s^{-1} and angle of incidence is 60° (w.r.t. surface normal). Impact direction is indicated by the arrow. Note the absence of granular residue, the pronounced trailing edge lips, and downrange impactor fragmentation damage. p/D ratio is 0.32.*

Figure 10. *Photomicrograph of impact site D80-05-123. Impact velocity was 10.5 km.s^{-1} and angle of incidence is 45°. Impact direction is indicated by the arrow. Note the almost circular footprint and lack of asymmetry between leading and trailing edge lips. p/D ratio is 0.48, indicating an almost hemispherical crater which would be indistinguishable from lower incidence impact craters.*

ORIGINAL PAGE IS
OF POOR QUALITY

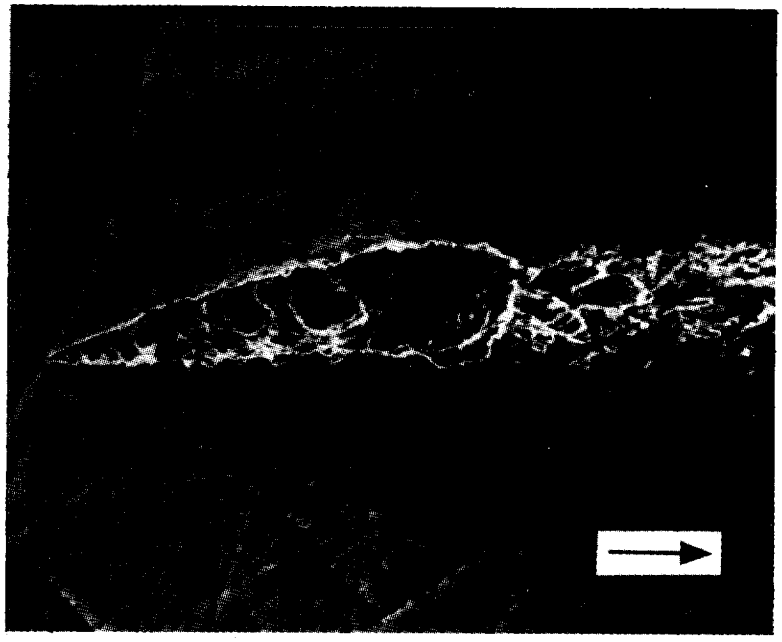

Figure 11. *Photomicrograph of impact site D79-01-02. Impact velocity is 5.7 km.s^{-1} and angle of incidence is 75° (w.r.t. surface normal). Impact direction is indicated by the arrow. Note the uprange gouge, central major "crater" and downrange impactor fragmentation damage.*

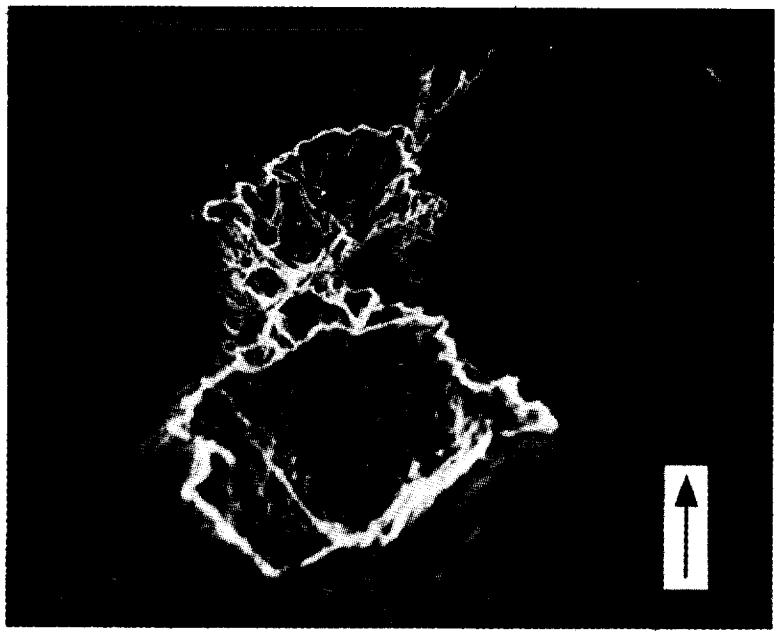

Figure 12. *Photomicrograph of impact site D79-03-04. Impact velocity is 12.5 km.s^{-1} and angle of incidence is 75° (w.r.t. surface normal). Impact direction is indicated by the arrow. Note that there is no uprange gouge, the central major "crater" is deep with significant lips. Downrange impactor fragmentation damage as still present.*

ORIGINAL PAGE IS
OF POOR QUALITY

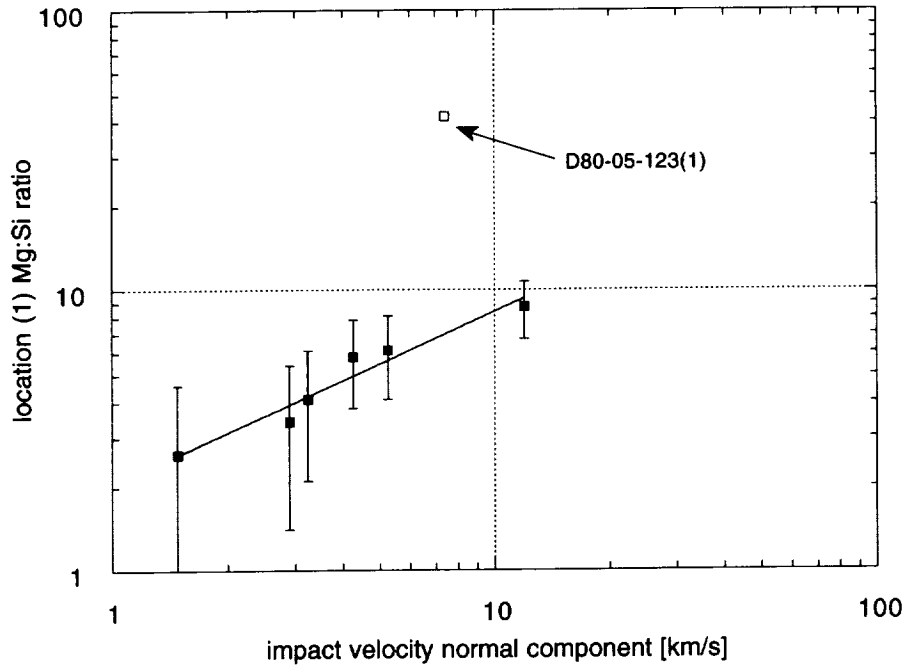

Figure 13. *Graph of location (1) residues Mg:Si ratio showing the increase of shock fractionation with increasing normal component of impact velocity (V_n).*

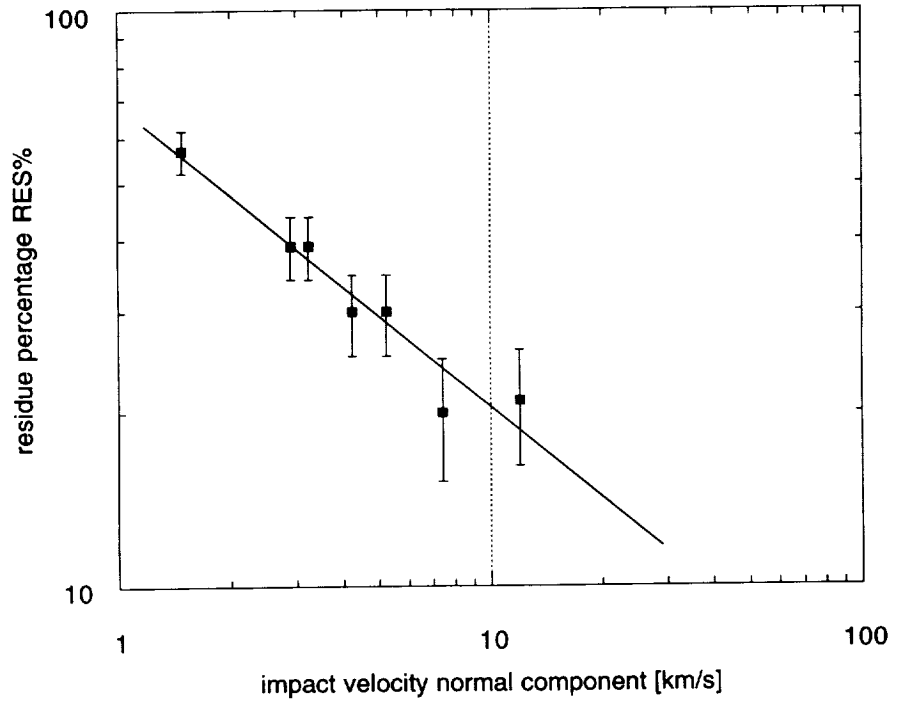

Figure 14. *Graph of location (1) residue percentage versus impact velocity normal component (V_n).*